Ultrastable Laser Wavelength Locking Technique Optimized for WMS-Based Methane Detection

Yaopeng Cheng, Fupeng Wang, Jinghua Wu, Rui Liang, Qiang Wang, Yubin Wei, Jiachen Sun, Qian Li, and Qingsheng Xue

***Abstract*—Fixed wavelength modulation spectroscopy (FWMS) featured as that wavelength is modulated around a constant value instead of a dynamic scanning ramp in the standard wavelength modulation spectroscopy (WMS). To eliminate the influence of center wavelength drift on absorption measurement in the FWMS system, a software-based proportional–integral–derivative (PID) controller is developed to lock the laser wavelength at methane line 1653.72 nm for CH_4 detection in this study. Moreover, two crucial parameters of PID, gain and integral time, are optimized to improve the laser wavelength locking performance. As a result, the laser wavelength is locked to the target CH_4 line with a 1σ fluctuation less than 406 kHz (better than 3.7×10^{-3}pm) with a robust 100% locking success rate, which is the best result reported so far to our knowledge. Based on the wavelength locked FWMS CH_4 sensor, linearity is tested to be $R^2 = 0.998$ in a low concentration range of 0–1000 ppm. The detection sensitivity is 52 ppb at 0.1 s and could be improved to 36 ppb if the integration time is extended to 1.4 s. Compared with standard WMS, CH_4 detection stability is improved by five times.**

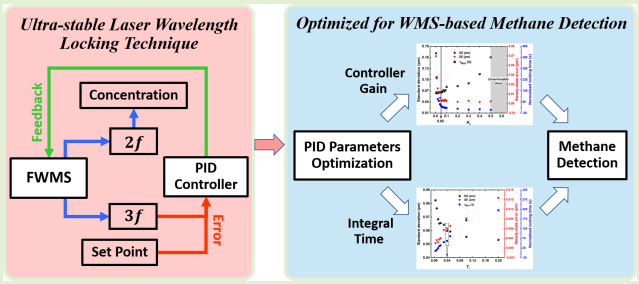

***Index Terms*— Laser wavelength locking, methane detection, proportional–integral–derivative (PID), wavelength modulation spectroscopy (WMS).**

I. Introduction

TRACE gas detection is indispensable across a wide range of industrial applications, such as food safety, medical diagnostics, combustion processes, and environmental monitoring [1], [2], [3], [4]. Tunable diode laser absorption spectroscopy (TDLAS), nowadays, is dominant among various gas detection techniques due to its robustness, long service life, high selectivity, and high sensitivity. In a direct absorption spectroscopy (DAS) system, there are generally two approaches to enhance its detection sensitivity. The straightforward one is to increase the absorption path length. On the one hand, cavity-enhanced absorption spectroscopy (CEAS) and cavity ring-down spectroscopy (CRDS) have demonstrated a high sensitivity performance [5], [6]. On the other hand, multipass cells are developed, leading to a minimum detection limit (MDL) of parts per million (ppm) or parts per billion (ppb) level for CH_4, C_2H_2, NH_3, and so on [7], [8], [9], [10], [11], [12]. In addition, the gas absorption lines in the mid-infrared (MIR) region are, in general, three orders of magnitude stronger than the ones in the near-infrared (NIR) band [13], [14]. Thus, MIR tunable light sources, such as interband cascade laser (ICL) and quantum cascade laser (QCL), have been employed in TDLAS-based systems [15], [16], [17], [18], [19]. Furthermore, the wavelength modulation spectroscopy (WMS) technique with lock-in amplifier is proposed to enhance the detection sensitivity by virtue of its excellent noise rejection performance. Thus, the WMS technique has been widely applied to all kinds of absorption spectroscopy trace gas sensing systems. Apart from the DAS, indirect absorption spectroscopy (IDAS) has

Manuscript received 31 January 2023; accepted 14 February 2023. Date of publication 24 February 2023; date of current version 31 March 2023. This work was supported in part by the National Natural Science Foundation of China under Grant 52001295 and Grant 62005267; in part by the Natural Science Foundation of Shandong Province under Grant ZR2020QF097 and Grant ZR2021QD140; in part by the Open Fund of State Key Laboratory of Applied Optics under Grant SKLAO2021001A12; in part by the Fundamental Research Funds for the Central Universities under Grant 202013024 and Grant 202065004; and in part by the Shandong Postdoctoral Innovation Program, Key Research and Development Program of Shandong Province, under Grant 2020CXGC010706. The associate editor coordinating the review of this article and approving it for publication was Dr. Qiang Wu. *(Corresponding author: Fupeng Wang.)*

Yaopeng Cheng, Jinghua Wu, Rui Liang, Qian Li, and Qingsheng Xue are with the Faculty of Information Science and Engineering, Ocean University of China, Qingdao 266100, China.

Fupeng Wang is with the Faculty of Information Science and Engineering, Ocean University of China, Qingdao 266100, China, and also with the State Key Laboratory of Applied Optics, Changchun Institute of Optics, Fine Mechanics and Physics, Chinese Academy of Sciences, Changchun 130033, China (e-mail: wfp@ouc.edu.cn).

Qiang Wang is with the State Key Laboratory of Applied Optics, Changchun Institute of Optics, Fine Mechanics and Physics, Chinese Academy of Sciences, Changchun 130033, China.

Yubin Wei is with the Laser Institute, Qilu University of Technology (Shandong Academy of Sciences), Jinan 250102, China.

Jiachen Sun is with the School of Information Science and Engineering and the Shandong Provincial Key Laboratory of Laser Technology and Application, Shandong University, Qingdao 266237, China.

Digital Object Identifier 10.1109/JSEN.2023.3246508

developed rapidly in recent decades such as photoacoustic spectroscopy (PAS) [20], [21], [22], [23], [24], [25], photothermal spectroscopy (PTS) [26], [27], [28], [29], and light-induced thermoelastic spectroscopy (LITES) [30], [31], [32]. In an IDAS-based experiment diagram, the WMS technique is also applicable and preferred. Therefore, great importance ought to be attached to the improvement of WMS technique since the WMS technique plays a vital part in both DAS and IDAS systems.

There are two main working modes for a WMS-based system: standard wavelength scanning mode (standard WMS) and fixed wavelength mode (FWMS). In the former one, a scanning ramp in low frequency is used to realize wavelength scanning with a certain bandwidth, which aims to cover one or more absorption lines of target gas. Meanwhile, a higher frequency sinusoidal signal is superimposed on the scanning ramp to modulate the laser source. Harmonic signals are generated from the interaction between the modulated light and target gas molecular and detected by a photodetector. Commonly, the 2nd harmonic signal is measured by a lock-in amplifier to retrieve the concentration of target gas. The advantages of standard WMS mode are apparent. First, the measured results are insensitive to the wavelength drift effect because you can always find the absorption center by aiming at the 2nd harmonic peak, and the influence of power drift concurrent with wavelength drift could be eliminated by the $2f/1f$ calibration technique [33]. In addition, more absorption-related information can be detected because the intact absorption line shape is scanned, for example, the gas concentration, pressure, and temperature. Thus, most of the WMS-based gas sensing systems prefer to choose the standard mode. However, because a low-frequency ramp is used to scan the line shape, there is merely one effective data point in a scanning cycle to predict gas concentration. This would reduce the response speed of gas sensor. Increasing the scanning frequency is an optional method for higher response speed, but this requires a lock-in amplifier to increase the 3-dB bandwidth of its low-pass filter so that the scanning frequency can pass smoothly without any signal reduction and distortion. Unfortunately, the 3-dB bandwidth is the pivotal parameter for lock-in amplifier to obtain a high signal-to-noise ratio (SNR) in which increasing the 3-dB bandwidth is equivalent to reducing SNR, that is to say, there is irreconcilable contradiction between response speed and noise rejection in the standard WMS mode. By contrast, in the fixed wavelength mode, theoretically speaking, the center wavelength of laser source is fixed at the absorption line center of target gas by a constant driving current. Then, a higher frequency sinusoidal signal is applied at the same time to realize the wavelength modulation around the center wavelength. Consequently, the 2nd harmonic output is a constant value (dc signal), which corresponds to the maximum of the 2nd harmonic curve measured in the wavelength scanning mode, and the output of this working mode is enough for applications that only aim to measure gas concentration. As a result, the FWMS mode has advantages as follows. First, the low-pass filter of lock-in amplifier can be further compressed because of the dc output, which is helpful to improve the SNR. Second, more effective data can be recorded in a given time instead of only one effective data point every scanning cycle in the standard WMS method. Then, the cumulative averaging algorithm can be further employed to enhance the SNR by reducing the random noise. Third, the nonlinearity of the wavelength response of laser sources was reported to distort the harmonic signals, bringing in undesired absorption-independent noise [34]. Obviously, the standard mode suffers from the influence of this kind of nonlinearity; however, the FWMS mode does not. Fourth, the thermal stability and service life of the laser diode are likely to be improved if the laser was driven by a relatively constant current instead of operating in a large dynamic range [35]. Finally, the fixed wavelength mode enables the system to make full use of the photodetected signal and the dynamic range of electronic circuits [35]. Therefore, the FWMS technique is selected to develop our CH_4 sensor in this study and can be extended to other gas detection.

However, the laser wavelength would drift with variations of ambient conditions in practice, especially the environmental temperature [36]. Moreover, the aging of the laser electronic components can cause drifts on wavelength as well [37], [38]. Such aging effects are uncontrollable, so a simple stabilization of the environmental parameters is yet insufficient. The intractable laser wavelength drift is prone to take a toll on the detection sensitivity of FWMS-based gas sensing systems. Therefore, an active wavelength locking technique is strongly required. In the field of laser technology, wavelength locking (mode locking) is usually needed and researchers have paid a lot of effort on it [39], [40], [41]. However, most of these strategies are not applicable to TDLAS-based gas sensing systems. As to the field of gas detection, a proportional–integral–derivative (PID) controller has been introduced to stabilize the laser wavelength at the absorption center [42]. However, to our knowledge, the influence of different PID parameters on the performance of wavelength locking has never been studied in a TDLAS-based gas sensing system.

In this article, we develop a PID-based negative feedback controller to lock the center wavelength of laser at the target gas absorption line, realizing a 100% locking success rate. In addition, the parameters of PID controller are evaluated in detail, further improving the stability of laser wavelength locking to an exciting level. The optimized laser wavelength locking technique is verified in an FWMS-based CH_4 sensing system, a sensitivity of 35 ppb at 1.4-s integration time, and linearity ($R^2 = 0.998$) in a low concentration range of 0–2000 ppm that are achieved. All the functions mentioned above are realized and optimized based on a LabVIEW-driven platform in this study. In the next step, efforts would be paid on transplanting the ultrastable laser wavelength locking technique to microcontroller units (MCUs) so that it can be easily applied to gas sensing systems.

II. Methodology

A. Principle of WMS

To explain the principle of our proposed wavelength locking technique used in the FWMS system, we have to briefly introduce the WMS strategy first. The basic process of WMS-based trace gas detection is shown schematically in Fig. 1. In a WMS

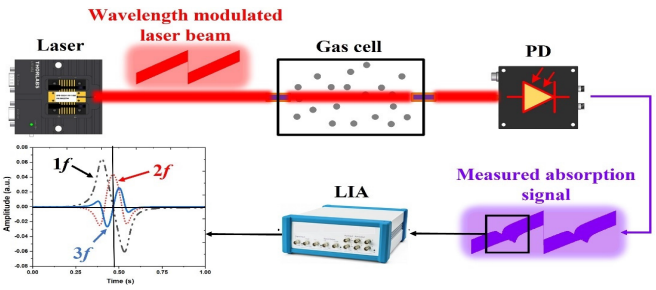

Fig. 1. Schematic of the WMS-based trace gas detection. PD: photodetector. LIA: lock-in amplifier. 1*f*: 1st harmonic. 2*f*: 2nd harmonic. 3*f*: 3rd harmonic.

system, light modulation can be readily achieved through the injection current modulation by virtue of the tunability and modulation capability of the distributed feedback (DFB) lasers. This procedure brings about the combined simultaneous modulation of the laser frequency (i.e., wavelength modulation) and laser optical power (i.e., intensity modulation). The modulated laser frequency response and intensity response can be, respectively, expressed as

$$\nu(t) = \nu_c(t) + \Delta\nu \cdot \cos(\omega t) \tag{1}$$

$$I_0(t) = I_c(t) + \Delta I \cdot \cos(\omega t - \Delta\varphi) \tag{2}$$

where $\Delta\nu$ is the frequency modulation depth that is the maximum excursion of $\nu(t)$ around $\nu_c(t)$ the central frequency of modulation, $I_c(t)$ denotes the optical intensity at the central frequency, ΔI is the intensity modulation amplitude, ω is the angular frequency of modulation, and $\Delta\varphi$ denotes the phrase shift between the frequency modulation and the intensity modulation. It is noteworthy that the frequency modulation is expected to probe the absorption information, while the intensity modulation is an unwanted side effect that distorts the harmonics and is hence usually referred to as residual amplitude modulation (RAM) in the literature [43], [44].

The WMS technique is based on the light absorption by the molecules of the target gas and the transmitted light follows the well-known Beer–Lambert law, namely:

$$I(\nu) = I_0(\nu) \cdot \exp\left[-S(T) \cdot g(\nu, \nu_0) \cdot P \cdot C \cdot L\right] \tag{3}$$

where $S(T)$ is the intensity of the transition line at temperature T, $g(\nu, \nu_0)$ is the absorption line shape function, P is the gas pressure, C is the concentration of target gas, L is the absorption path length, and $I_0(\nu)$ denotes the intensity of incident light. As shown in Fig. 1, the wavelength-modulated laser beam is tuned to cover the absorption line of target gas. After passing through the gas cell, the photodetected signal contains absorption-induced harmonics. The specified harmonic signal can be demodulated by means of synchronous detection using a lock-in amplifier. The 1st, 2nd, and 3rd harmonics can be written, respectively, as

$$\begin{aligned} V_1 &= I_c H_1 \cos(\omega t)\, S(T)\, PCL \\ &\quad + \frac{1}{2}\Delta I H_0 \cos(\omega t - \Delta\varphi)\, S(T)\, PCL \\ &\quad + \frac{1}{2}\Delta I H_2 \cos(\omega t + \Delta\varphi)\, S(T)\, PCL \end{aligned} \tag{4}$$

$$\begin{aligned} V_2 &= I_c H_2 \cos(2\omega t)\, S(T)\, PCL \\ &\quad + \frac{1}{2}\Delta I H_1 \cos(2\omega t - \Delta\varphi)\, S(T)\, PCL \\ &\quad + \frac{1}{2}\Delta I H_3 \cos(2\omega t + \Delta\varphi)\, S(T)\, PCL \end{aligned} \tag{5}$$

$$\begin{aligned} V_3 &= I_c H_3 \cos(3\omega t)\, S(T)\, PCL \\ &\quad + \frac{1}{2}\Delta I H_2 \cos(3\omega t - \Delta\varphi)\, S(T)\, PCL \\ &\quad + \frac{1}{2}\Delta I H_4 \cos(3\omega t + \Delta\varphi)\, S(T)\, PCL \end{aligned} \tag{6}$$

where H_n is the nth Fourier expansion coefficient of the absorption line shape function. The concentration of the target gas is retrievable since the harmonic signal is directly proportional to the absorption. Commonly, the detection is shifted to a higher frequency, typically the 2nd harmonic, where the $1/f$ noise is reduced and the amplitude of the harmonic signal does not decrease too much with the rise of the harmonic order.

B. Laser Wavelength Locking Strategy

Theoretically, in pure wavelength modulation free from RAM, the even-order harmonic curves are symmetric about the absorption line center, whereas the odd harmonic values are zero at the center of the absorption line as shown in harmonic curves of Fig. 1. It is customary to use the zero intersection of the 3rd harmonic signal as a reference point to determine the absorption line center. However, as shown in the zoomed inset of Fig. 2(a), a slight shift between the zero intersection and the absorption line center will occur as long as the laser has RAM. As a result, the laser cannot be locked exactly to the line center if still using the zero intersection as the reference point. Thus, we have to refind the true reference point from the 3rd harmonic signal for wavelength locking. The true reference point is determined as follows. Considering that the 2nd and 3rd harmonic curves can be collected synchronously as shown in Fig. 2(a) and the symmetry axis of the 2nd harmonic curve corresponds to the centerline of absorption profile, we choose the intersection of this symmetry axis and the 3rd harmonic curve as the reference point ["set point" in Fig. 2(a)]. To verify the feasibility of using this "set point" for wavelength locking, a preliminary experiment is performed based on a standard WMS mode CH_4 sensing system. In this experiment, a constant concentration of CH_4 sample is provided to hold stable gas absorption, and the 2nd and 3rd harmonic signals are saved synchronously for 3 h. The 2nd harmonic amplitude and 3rd harmonic "set point" are calculated and recorded, which are plotted in Fig. 2(b) and (c), respectively. As shown in Fig. 2(b), the 2nd harmonic amplitude drifts due to several reasons, including laser power drift, laser wavelength drift, and other absorption-independent fluctuations. However, the value of the "set point" keeps constant as shown in Fig. 2(c), which means that the

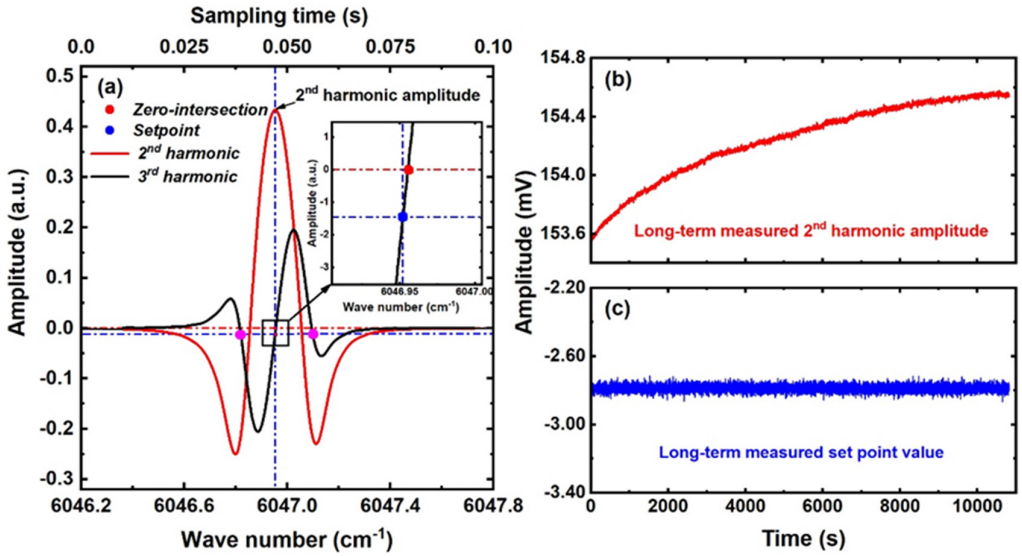

Fig. 2. (a) Representative 2nd and 3rd harmonic curves measured under RAM effect. (b) Long-term measured 2nd harmonic amplitudes in a 3-h period. (c) Long-term measured SPs in a 3-h period.

determined "set point" is steady enough a reference point to lock the laser wavelength at the absorption line center.

As explained above, the "set point" has been identified successfully in the first step. If we keep measuring the 3rd harmonic signal and comparing it with the "set point" and then manage to make the detected 3rd harmonic value approach the "set point" by adjusting the laser driving current dynamically, the laser wavelength would be stabilized at the absorption center of target gas. This process is termed laser wavelength locking, and a PID controller is usually employed in this process. At any given moment, the PID controller calculates the error signal by subtracting the real-time measured 3rd harmonic signal (RM) from the "set point" value (SP) and then feedbacks a correction value, i.e., the manipulated variable (MV), in a bid to control the RM to approach the SP. The theoretical model of a PID controller is expressed as follows:

$$u_p(t) = K_c \cdot e(t) \tag{7}$$

$$u_I(t) = u_I(t-1) + \frac{K_c}{T_i}\left(\frac{e(t)+e(t+1)}{2}\right)\Delta t \tag{8}$$

$$u_D(t) = -K_c \frac{T_d}{\Delta t}\left(RM(t) - RM(t-1)\right) \tag{9}$$

where $u_p(t)$, $u_I(t)$, and $u_D(t)$ are proportional term, integral term, and derivative term, respectively; K_c, T_i, and T_d are three important parameters of every PID controller, called controller gain, integral time, and derivative time, respectively; $e(t)$ is the real-time calculated error signal; and Δt is the sampling time. The summation of these three terms constitutes the MV as a feedback value to adjust the laser driving current as expressed in the following equation:

$$MV = u_P(t) + u_I(t) + u_D(t). \tag{10}$$

III. Experimental Setup

Most of the current TDLAS-based CH_4 sensors are developed by exploiting the overtone band of CH_4 near 1650 nm due to the matured semiconductor laser and detector technologies in the NIR region. Fig. 3 shows the simulated 1-ppm CH_4 absorption coefficient in the range of 6020–6070 cm^{-1} according to the HITRAN database. Considering that H_2O, CO_2, and NH_3 are the major interfering components in the 1650-nm band, absorption coefficients of these three species are also simulated in Fig. 3. Water vapor concentration in the tropics can reach up to 4%; the maximum allowable average concentration of CO_2 for human breathing is 1.5% [45] and the maximum allowable concentration of indoor NH_3 is 0.2 mg/m^3 (≈0.26 ppm) according to the Chinese standard GB/T1883-2002. For a better comparison between the multispecies in the same y-scale, 1-ppm CH_4, 4% H_2O, 2000-ppm CO_2, and 10-ppm NH_3 are simulated in Fig. 3. From Fig. 3, 1653.72 nm (6046.96 cm^{-1}) and 1650.96 nm (6057.08 cm^{-1}) are two ideal choices for CH_4 detection. However, 1650.96 nm is beyond the operating range of the current laser diode in our laboratory, so 1653.72 nm is chosen to validate and optimize the process of laser wavelength

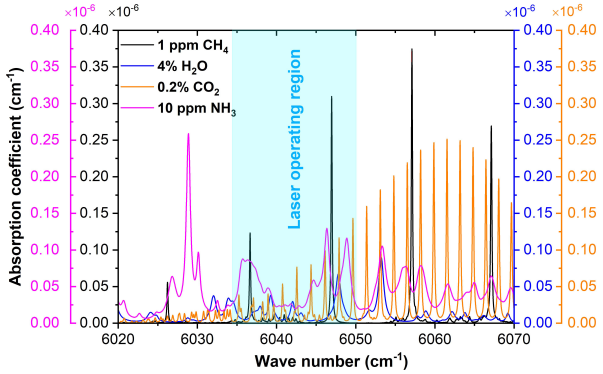

Fig. 3. Simulated absorption coefficient from 1648 to 1660 nm of 1-ppm CH_4, 4% H2O, 2000-ppm CO_2, and 10-ppm NH3 at 1 bar and 296 K. Shadow zone: wavelength output range of the current laser diode in our laboratory is 1652–1657 nm.

locking in this study. Accordingly, a DFB semiconductor laser (DFB-1653-N-SM, Wuhan 69 Sensing Tech, China) emitting at 1653 nm is utilized as the light source in the experimental system. The experimental setup is configured, as shown in Fig. 4. A LabVIEW-driven DAQ card (USB 6361, National Instruments, Austin, TX, USA) is employed, based on which functions, including signal generation, data acquisition, lock-in detection, and PID controlling, are programmed in LabVIEW language to serve this study. First, a 4-kHz, peak-to-peak 0.6-V sinusoidal signal is generated from the AO-0 port of DAQ card to realize the wavelength modulation. Besides, a 1.86-V offset is added to the sinusoidal signal to roughly tune the laser center wavelength to the CH_4 absorption center. The voltage signal from the AO-0 port is transmitted into current to drive the DFB laser by a commercial driver (LDC501, Stanford Research Systems, Sunnyvale, CA, USA) with a 25-mA/V conversion ratio; meanwhile, the laser's operating temperature is controlled by LDC501 as well to 29.6 °C. The laser output beam is split by a 1×2 coupler and coupled into a sensing cell (3-m optical path length Herriott gas cell) and a reference cell (a miniatured gas chamber integrated with PD #2 filled with constant concentration CH_4). The transmitted light is converted into the current signal by two fiber-coupled photodetectors PD #1 and PD #2. The output photocurrent from PD #1 and PD #2 is transmitted into a voltage signal by transimpedance amplifier (TIA) and then recorded by two analog-to-digital converter (ADC) channels (AI-0 and AI-1) of the DAQ card, respectively. The ADC-collected signals are subsequently processed by the LabVIEW-based software platform. The absorption signal from the sensing cell is demodulated by LIA #1 to obtain the 2nd harmonic signal for methane concentration calculation, while the absorption signal from the reference cell is demodulated by LIA #2 to extract the 3rd harmonic signal for wavelength locking. As demonstrated in Section II-B, the 3rd harmonic signal acts as an input to the PID controller for laser wavelength locking operation. In the experiments, the CH_4 sample gas used in the sensing cell is supplied by a gas mixing system, comprised of a customized mixing chamber, two flowmeters, 99.999% pure nitrogen, and 0.1% methane gas.

IV. Experiment Results

Based on the experiment system as demonstrated above, a PID controller is developed and optimized to realize the ultrastable laser wavelength locking function. The detailed procedures for the realization of laser wavelength locking are introduced in this Section IV-A. The laser wavelength locking performance is evaluated and compared by adjusting the PID parameters in this Section IV-B. The long-term stability of the laser wavelength locking is investigated in Section IV-C. Finally, the gas detection performance of the optimized laser wavelength locked WMS system is assessed through a CH_4 concentration detection experiment in Section IV-D.

A. Realization of the Laser Wavelength Locking

In the very beginning, before turning on the FWMS system, a period of standard wavelength scanning mode is performed in 10-Hz scanning frequency so that we can determine the SP value in advance following the method introduced in Section II-B. As a result, the SP is measured to be −2.8 mV, which means that the RM value should be −2.8 mV if the laser wavelength is accurately locked to the center of CH_4 absorption line. However, as described in the second paragraph of Section III, a 1.86-V offset is applied to LDC501 to roughly set the laser wavelength close to the CH_4 absorption line center, but not precisely. As a result, the RM (red triangle in Fig. 5) is far away from the SP of −2.8 mV in the beginning. Fig. 5 shows the laser wavelength locking process from turning on the PID controller. The difference between the initial measured 3rd harmonic value and the SP is calculated as initial error δ_{in}. At this moment as labeled in a red triangle, the PID controller is turned on, and the RM starts to approach the SP. When the RM arrives at the SP of −2.8 mV, it means that the laser wavelength has been locked to the CH_4 absorption center at 1653.72 nm. With the feasibility validated, it is time to quantitatively evaluate the laser wavelength locking performance under different PID parameters. In the end, an optimal group of PID parameters is expected to achieve an ultrastable laser wavelength locking result.

The blue arrow marked in Fig. 5 denotes the moment that the RM first reached the SP. The time from turning on the PID controller to the arrival at the SP is defined as the locking time τ_L. However, the initial error δ_{in} from every locking operation may be slightly different in practice, so the locking time τ_L cannot represent the locking efficiency authentically. To provide a fair comparison, the locking time τ_L is normalized by the initial error δ_{in} to define the normalized locking time τ_{Nor} for the following optimization, indicating the efficiency of laser wavelength locking. In addition to the efficiency, stability and accuracy are still evaluated in the optimization study. As shown in Fig. 5, a hundred seconds after it first reached the SP, and the RM is practically steady near the SP. From this point on, the 3rd harmonic signal is recorded for 5 min, as highlighted in a yellow rectangle in Fig. 5. Based on the 5-min collected data, a statistical analysis is performed to calculate the mean value and standard deviation (SD). We use the SD to indicate the stability of wavelength locking. As for the accuracy, steady-state error (SE) is calculated as the difference between the mean value and the preset SP value, which reveals the deviation of the locked wavelength away from the target wavelength [46]. Note that the SD and the SE appeared in Section IV-B are all converted from voltage to picometer (pm) unit via a transfer coefficient between the 3rd harmonic signal and the laser wavelength. The method to determine the transfer coefficient is introduced in detail in the Appendix.

B. Optimization of the Wavelength Locking Performance

In most cases, the laser wavelength locking technique is proposed to reduce the influence from minor and flat disturbances of environment. In such a condition, the controller gain and integral time are pivotal to the locking performance, yet the derivative time can be dismissed since it is used to mitigate sudden change and severe fluctuation. In this

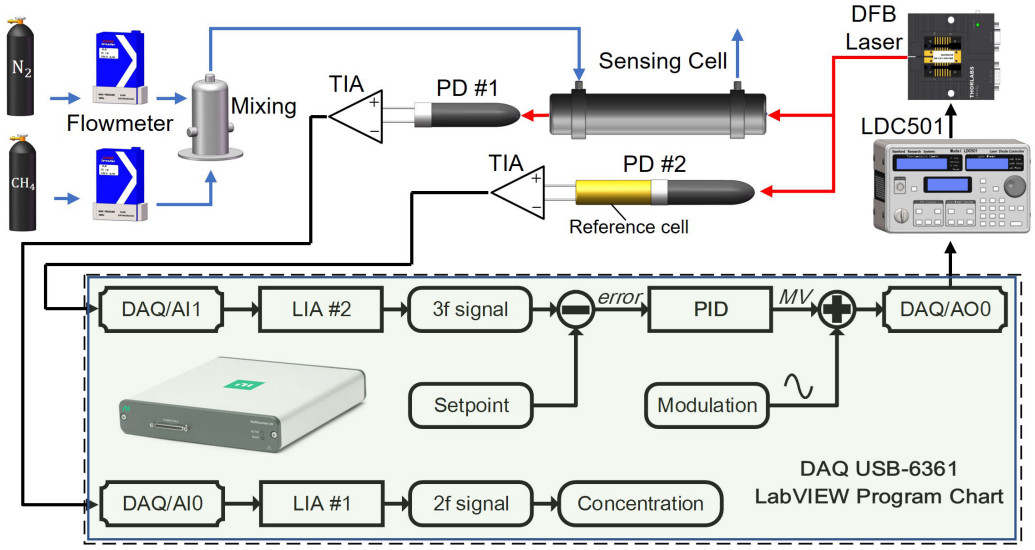

Fig. 4. Schematic of PID-based laser wavelength locking and methane detection system. TIA: transimpedance amplifier. DAQ: data acquisition card. PD: photodetector. LIA: lock-in amplifier. PID: proportional–integral–derivative controller. MV: manipulated variable.

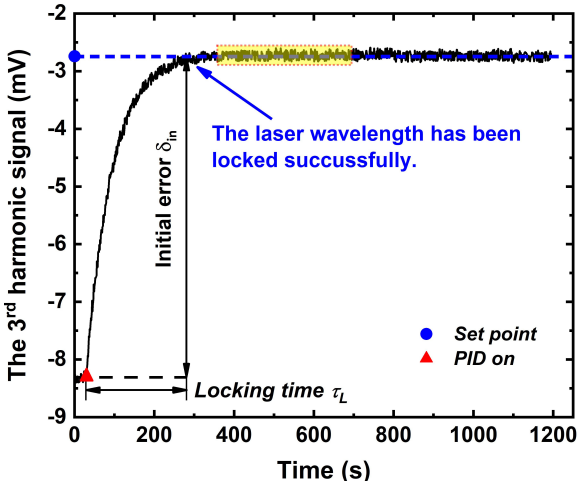

Fig. 5. RM after turning on the PID controller (low K_c was chosen to obtain this figure so that the dynamic process can be displayed easily).

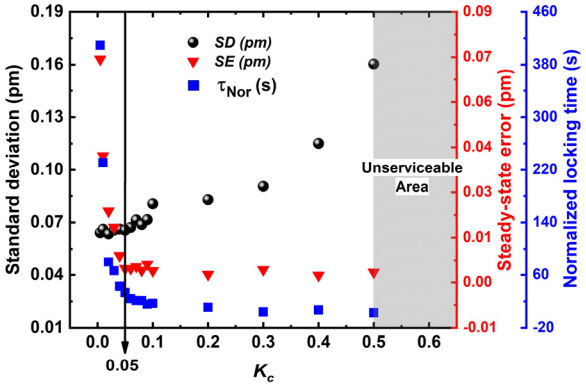

Fig. 6. Relationship between the laser wavelength locking performance and the PID controller gain. SD: standard deviation. SE: steady-state error. τ_{Nor}: normalized locking time.

second, wavelength locking efficiency, stability, and accuracy are quantitatively analyzed under different PID parameters, including the controller gain and integral time.

In the first step, the PID controller gain is changed from 0.01 to 0.5 to evaluate its influence on the result of laser wavelength locking; meanwhile, another two parameters of PID controller, integral time and derivative time, are set to be 0.016 and 0.001, respectively. Fig. 6 shows the relationship between the wavelength locking performance and controller gain K_c. As K_c decreases, the SD falls, indicating that the stability of locking is improved. However, due to the inelim-inable noise of the circuits, the SD approaches a constant value with further decreasing K_c less than 0.1. In addition, both the SE and τ_{Nor} take on an inverse relationship with K_c, which means that raising K_c is conducive to improve the locking accuracy and efficiency. As a result, K_c is optimized to be 0.05, considering that the SD does not improve greatly with K_c less than 0.1 and the SE and τ_{Nor} escalate badly when K_c is tuned below 0.05.

It should be noted that the PID controller will be disabled if the controller gain surpasses the upper limit of 0.5 in our experiment, the laser wavelength locking fails in the shadow area in Fig. 6. As shown in Fig. 2(a), there are two interference points that have the same value with the SP on both sides of the "set point." If the controller gain is set larger than 0.5, the initial feedback MV of PID will be so large that the RM jumps to the region beyond the interference points. However, the monotonicity nearby the interference points is contrary to the "set point" area, which would disable the PID controller. To deal with this problem, a threshold is measured in advance and added to the output of PID controller to make sure that the feedback MV is always within a prescribed boundary. As a result, a 100% laser wavelength locking success rate is achieved in our experiment.

The relationship between the laser wavelength locking performance and integral time T_i is shown in Fig. 7. In the experiment of this section, the controller gain is fixed at

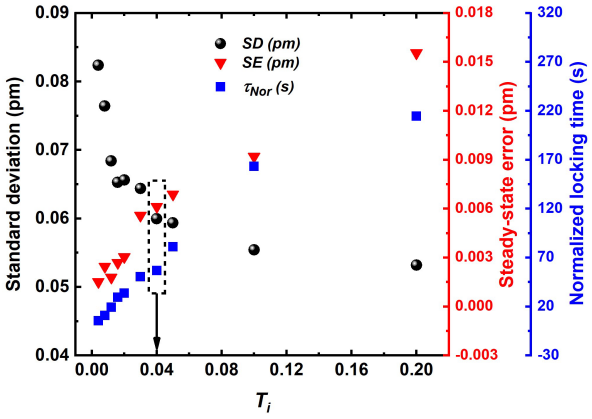

Fig. 7. Relationship between the laser wavelength locking performance and the integral time of the PID controller. SD: standard deviation. SE: steady-state error. τ_{Nor}: normalized locking time.

0.05 and the derivative time is still 0.001. T_i rises from 0.004 to 0.2, causing a regular change in the laser locking performance. On the one hand, the larger T_i brings about the smaller SD, i.e., the higher stability. However, the stability is not enhanced remarkably with T_i more than 0.04. On the other hand, T_i is proportionate to the SE and τ_{Nor}, which implies that it is beneficial to reduce T_i for high accuracy and efficiency. Overall, T_i is finalized to be 0.04 so that the three sides of the laser wavelength locking performance are in a satisfied level in the meantime.

To summarize briefly, smaller controller gain and extended integral time would lead to lower SD but higher SE and τ_{Nor}. According to this evaluation, the parameters of PID controller are optimized as: the controller gain is 0.05, the integral time is 0.04, and the derivative time is 0.001. Based on the parameters, we expect to achieve an ultrastable laser wavelength locking result.

C. Long-Term Stability of the Laser Wavelength Locking

Since the laser wavelength locking technique is developed to eliminate the wavelength drift of FWMS system, a specified experiment is carried out to study the long-term stability of the laser wavelength locking. The 3rd harmonic signal is recorded for 3 h to assess the wavelength drift of FWMS free running mode and the stability of laser wavelength locked mode. For better comparison of wavelength stability, the measured 3rd harmonic value is transferred into picometer by the method introduced in the Appendix. In the laser wavelength locked mode, three groups of PID parameters are applied for comparison.

When the system works in the pure FWMS mode with the PID controller turned off, an obvious wavelength drift is observed, as shown in Fig. 8(a). In the period of 3-h data collection, an approximately 2.66-pm wavelength drift occurs. Based on our experiment experience, the wavelength always drifts to a single direction in a few hours. However, considering the environmental fluctuation, it would drift back and forth if we extend the time window to several days. Afterward, the PID controller is turned on and the laser wavelength locking function is activated. The laser wavelength locked results from three groups of PID parameters are shown in Fig. 8(b)–(d). In this long-term experiment, τ_{Nor} is far smaller than the detection time, so the parameter of τ_{Nor} is dismissed in comparison. Locking stability and accuracy (i.e., the SD and SE) is investigated and compared. First, the PID parameters are set as $K_c = 0.4$, $T_i = 0.016$, and $T_d = 0.001$, and its results are plotted in Fig. 8(b); the SD and SE turn out to be 4.47×10^{-2} and 3.47×10^{-4} pm, respectively. Second, the parameters are changed to $K_c = 0.05$, $T_i = 0.016$, and $T_d = 0.001$ and reconduct the laser wavelength locking operation. As a result, the SD falls nearly by half to 2.41×10^{-2} pm and the SE slightly increases to 4.06×10^{-4} pm, as shown in Fig. 8(c). In the last group of parameters as $K_c = 0.05$, $T_i = 0.04$, and $T_d = 0.001$, the SD is reduced significantly to 3.7×10^{-3} pm, while the SE sharply grows to 2.06×10^{-3} pm, as shown in Fig. 8(d). Fortunately, it is the SD instead of the SE that plays a decisive role in the sensitivity of an FWMS-based gas sensing system because the laser wavelength fluctuates around the target CH_4 line corresponding with the SD value, contributing to the 1σ of the 2nd harmonic signals and consequently undermining the sensitivity and MDL. Therefore, the last group of PID parameters used in Fig. 8 is chosen as the best option and applied to the methane detection experiment in Section IV-D. Comparing the results of Sections IV-B and IV-C, the conclusions are consistent. The optimized PID parameters prove its high stability in a long-run wavelength locking. The laser wavelength is locked to the target CH_4 line with a fluctuation less than 406 kHz (better than 3.7×10^{-3} pm), which is the best result reported so far to our knowledge.

D. CH_4 Detection Based on the Wavelength Locked FWMS System

After the optimal PID parameters are determined, the experiment system as shown in Fig. 4 can work in three modes: standard WMS mode, FWMS mode, and wavelength locked FWMS mode. In the standard WMS mode, a 10-Hz scanning sawtooth superimposed with a 4-kHz sinusoidal signal from channel AO-0 is used to drive the DFB laser by LDC501. As a result, a 2nd harmonic curve is measured in every scanning cycle of 0.1 s so that the 2nd harmonic amplitude is collected with a 10-sample/s rate for absorption calculation. In the FWMS and wavelength locked FWMS modes, the 2nd harmonic output of lock-in amplifier is a dc value instead of a 2nd harmonic curve. So, the sampling rate is no longer limited by the 10 Hz scanning frequency and averaging algorithm could be applied as well. However, due to the limited computational capacity of our software diagram, the averaging algorithm has not been implemented in the system, as the extensive averaging time would cause the PID locking loop to collapse. On the other hand, to give a fair comparison with the standard WMS mode, the sampling rate of 2nd harmonic dc value is also set 10 sample/s in the wavelength locked FWMS mode.

Fig. 9 shows the measured results in different CH_4 concentration when the system works in the wavelength locked FWMS mode. Fig. 9(a) presents the result of the consistency analysis by increasing and decreasing the CH_4 concentration in the range of 50 to 1000 ppm. A linear fit is performed

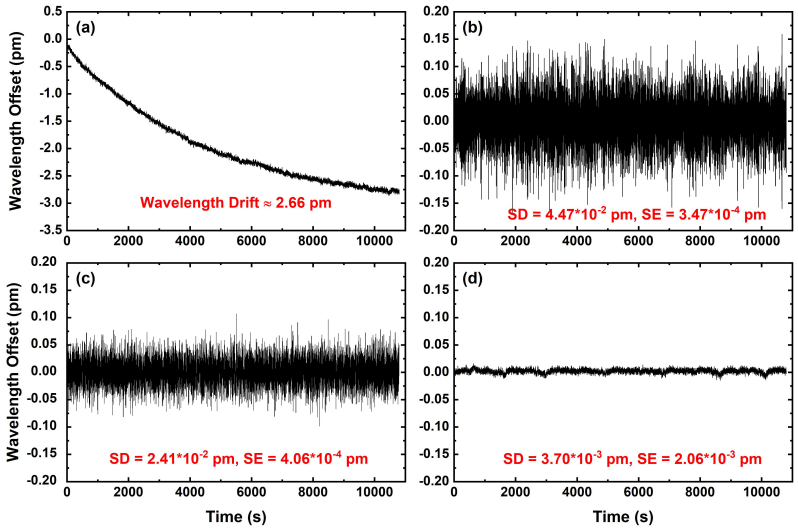

Fig. 8. Laser wavelength offset from the absorption line center in 3-h detection. (a) Free running. (b) $K_c = 0.4$, $T_i = 0.016$, and $T_d = 0.001$. (c) $K_c = 0.05$, $T_i = 0.016$, and $T_d = 0.001$. (d) $K_c = 0.05$, $T_i = 0.04$, and $T_d = 0.001$.

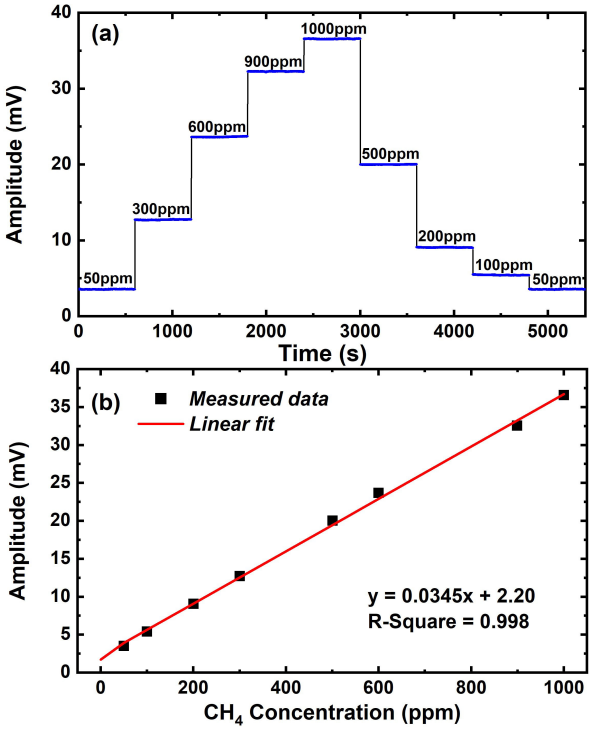

Fig. 9. Methane detection based on the ultrastable laser wavelength locked FWMS system. (a) Second harmonic amplitudes in different CH4 concentrations. (b) Linear response of methane detection.

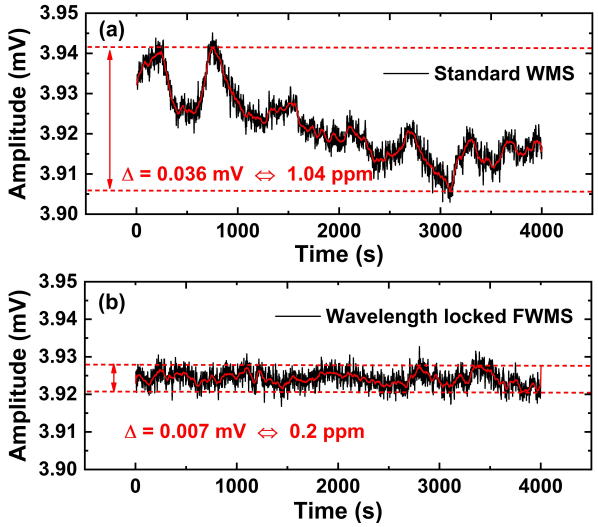

Fig. 10. Comparison of CH4 detection stability between (a) standard WMS mode and (b) wavelength locked FWMS mode.

and an R-square of 0.998 is achieved as depicted in Fig. 9(b), and a sensitivity of 34.5 μV/ppm is realized. In addition to the basic linearity test, the wavelength locked FWMS mode is expected to have better stability over standard WMS mode in our opinion. So, a comparative experiment is conducted between the standard WMS and wavelength locked FWMS modes based on the system in Fig. 4. In the experiment, 50 ppm CH_4 sample is continuously measured over 1 h in both modes, respectively, the results are displayed in Fig. 10. A maximum drift of 1.04 ppm is observed in standard WMS mode, which is equivalent to 2.1% drift in a concentration of 50 ppm. However, only 0.2 ppm drift is measured in the wavelength locked FWMS mode, and the stability is improved by 5 times.

As mentioned in the first paragraph of this section, the averaging algorithm has not yet applied to further improve the detection sensitivity due to the running limitation of software program. To explore the best sensitivity in FWMS mode benefited from the optimized ultrastable wavelength locked system, a commercial lock-in amplifier (MFLI, Zurich Instrument, Zürich) is temporarily adopted instead of the LIA#1 in Fig. 4 to measure the CH_4 concentration in sensing cell so that a large amount of data can be saved and averaged. In a concentration of 50 ppm CH_4 sample, the measured result is recorded over 5 minutes with a sampling rate of 1674 Sample/s. Based on the collected data, the Allan–Werle deviation analysis is performed to investigate the minimum noise level. As shown in Fig. 11,

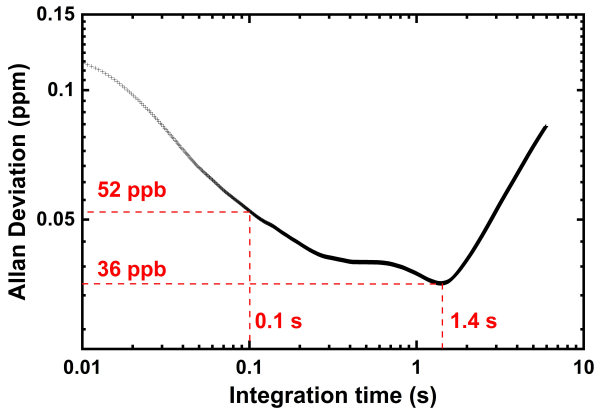

Fig. 11. Allan deviation analysis.

the Allan deviation indicates that the sensitivity is 52 ppb at 0.1-s integration time and can be improved to 36 ppb if the integration time is extended to 1.4 s, and the instrumental drift dominates later on.

V. Discussion

An ultrastable laser wavelength locking technique is developed and validated in a methane detection system. To sum up, this article mainly talks about two contents. One is the PID optimization process, in which we find out how different PID parameters affect the laser wavelength locking stability, accuracy, and efficiency. Based on these conclusions, we can set PID parameters reasonably according to different application scenarios. For example, if the environmental factors change violently, then higher K_c and lower T_i should be set so that the PID controller can timely respond to the violent wavelength fluctuations. If the environment drifts slowly, then lower K_c and higher T_i should be fine because PID controller does not need high response speed in this condition. The laboratory environment belongs to the latter, so K_c and T_i are optimized to 0.05 and 0.04 in this study, respectively. As a result, the laser wavelength is stabilized to a great level with a 1σ fluctuation less than 406 kHz (better than 3.7×10^{-3} pm). Another important content in this article is to study the improvement on CH_4 detection in an FWMS-based system. As the laser wavelength is always stabilized at the CH_4 absorption line center, the influence from wavelength drift can be eliminated. As a result, the drift of CH_4 detection coming from the wavelength drift can be suppressed as well. Compared with the standard WMS system, CH_4 detection stability is improved by five times by the wavelength locked FWMS system. Furthermore, the low-pass filter of lock-in amplifier can be further compressed, and in the experiment of Fig. 11, the lock-in bandwidth of MFLI is compressed to 10 Hz. In addition, the Allan deviation results show that the CH_4 detection sensitivity is 52 ppb at 0.1-s integration time and could be improved to 36 ppb if the integration time was extended to 1.4 s. We list a series of recently published studies about CH_4 detection in Table I for comparison. This work requires the shortest integration time while reaching the sub-ppm level sensitivity. The comparison shows that the advantage of wavelength locking technique is very obvious.

TABLE I
Comparison Among Recently Reported WMS-Based CH_4 Sensors

Gas	Laser wavelength	Sensitivity	Ref.
CH_4	1653.7 nm	52 ppb@0.1 s 36 ppb@1.4 s	This
CH_4	3.325 μm	0.5 ppm@2 s	[47]
CH_4	2334 nm	30 ppb@50 s	[48]
CH_4	1653.7 nm	56 ppm@150 s	[49]
CH_4	1684 nm	23 ppb@100 s	[50]
CH_4	1653.7 nm	2.66 ppm@273.8s	[51]

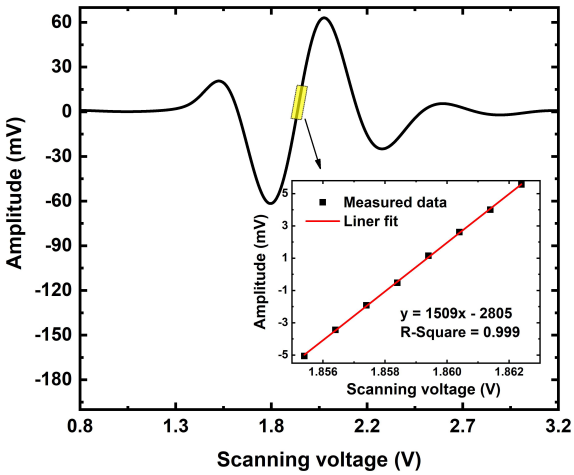

Fig. 12. Third harmonic curve of the reference cell acquired from the wavelength-scanning WMS mode. Inset: dependence of the 3rd harmonic signal amplitude on the voltage offset of the laser scanning ramp.

Limitations still exist in this study. First, considering the interference from H_2O and CO_2 on CH_4 detection, 1650.96 nm may be a little better choice compared with 1653.72 nm employed in this wavelength locked study. However, 1653.72 nm would also be a good choice for a standard WMS system in which intact harmonic curves are expected because weak CH_4 absorption peaks close to 1650.96 nm would distort the baseline of harmonic curves if 1650.96 nm is chosen in a standard WMS system. Second, the stability of locked wavelength analyzed in this study is calculated by 3rd harmonic signal as demonstrated in the Appendix instead of measuring it directly by wavemeter or etalon. The reason is that measuring wavelength stability in such high level of sub-picometer is a complicated work in itself. From another perspective, the Appendix demonstrates a high-precision method for measuring wavelength stability. Third, limited by the computational capacity of our software diagram, the averaging algorithm has not been applied to the system, as the extensive averaging time would make the PID locking loop collapse.

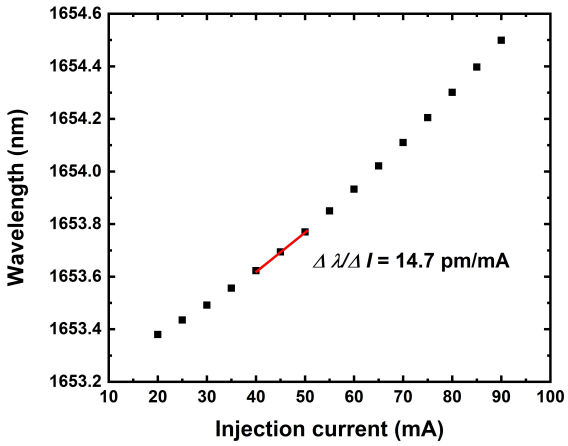

Fig. 13. Wavelength response toward driving current measured at a laser operating temperature of 29.6 °C.

In the future study, we will make efforts to optimize the software program so that averaging algorithm can be added into the system without breaking the PID controlling loop. In addition, bandpass filter circuit and gain circuit are expected in front of DAQ to increase the dynamic range of useful signal. In the last resort, all functions displayed in the dashed box of Fig. 4 should be migrated to an MCU for convenient application in engineering.

Appendix

In this section, the transfer coefficient between the 3rd harmonic signal and the laser wavelength ($\Delta A_{3f}/\Delta\lambda$) is elaborated in depth. In the first step, let us first figure out the transfer coefficient between the 3rd harmonic signal and the voltage offset of the laser scanning ramp ($\Delta A_{3f}/\Delta V$). As demarcated by a yellow rectangle in Fig. 12, the 3rd harmonic signal only fluctuates marginally at the center of the 3rd harmonic curve since the laser wavelength is locked at the absorption line center by the PID controller. Thus, the voltage offset of laser scanning ramp from 1.855 to 1.863 V is chosen, and the center of the 3rd harmonic curve is measured correspondingly. A liner fit is performed with an R-square of 0.999 and $\Delta A_{3f}/\Delta V$ is equal to 1509 mV/V.

In practice, the voltage of laser scanning ramp is converted into current by the LDC501 with a transfer coefficient ($\Delta I/\Delta V$) of 25 mA/V to drive the laser. Thus, the converted driving current is from 46.375 to 46.575 mA. The wavelength response toward the driving current at 29.6 ° laser operating temperature is measured in advance, as shown in Fig. 13. Although the wavelength response shows a nonlinear relationship in a broad current range, in a narrow range close to the CH_4 absorption center, the wavelength response ($\Delta\lambda/\Delta I$) can be described by its linear approximation and is derived to be 14.7 pm/mA. Finally, $\Delta A_{3f}/\Delta\lambda$ can be deduced as follows:

$$\frac{\Delta A_{3f}}{\Delta\lambda} = \frac{\Delta A_{3f}}{\Delta V} \Big/ \frac{\Delta I}{\Delta V} \Big/ \frac{\Delta\lambda}{\Delta I} = 4.106 \text{ mV}/\text{pm} \quad (11)$$

by which the SD and SE of the 3rd harmonic signal can be successfully converted from voltage to picometer unit. Therefore, during the laser wavelength locked period, the laser wavelength can be reflected by the 3rd harmonic signal due to its quantitative relationship with the 3rd harmonic signal.

Declaration of Competing Interest

The authors declare no conflicts of interest on this study.

References

[1] P. Puligundla, J. Jung, and S. Ko, "Carbon dioxide sensors for intelligent food packaging applications," *Food Control*, vol. 25, no. 1, pp. 328–333, May 2012.

[2] M. Jahjah et al., "A compact QCL based methane and nitrous oxide sensor for environmental and medical applications," *Analyst*, vol. 139, no. 9, p. 2065, 2014.

[3] M. E. Webber, J. Wang, S. T. Sanders, D. S. Baer, and R. K. Hanson, "In situ combustion measurements of CO, CO_2, H_2O and temperature using diode laser absorption sensors," *Proc. Combustion Inst.*, vol. 28, no. 1, pp. 407–413, Jan. 2000.

[4] G. Wysocki et al., "Dual interband cascade laser based trace-gas sensor for environmental monitoring," *Appl. Opt.*, vol. 46, no. 33, p. 8202, Nov. 2007.

[5] H. Zhang, J. Luo, S. Hou, Z. Xu, J. Evans, and S. He, "Incoherent broadband cavity-enhanced absorption spectroscopy for sensitive measurement of nutrients and microalgae," *Appl. Opt.*, vol. 61, no. 12, p. 3400, Apr. 2022.

[6] C. Cheng, S. Liu, H. Qi, P. Hu, P. Ye, and S. Pan, "Optical-feedback cavity ring-down spectroscopy for NO_2 extinction coefficient measurement using a continuous wave laser diode," *Appl. Opt.*, vol. 61, no. 9, p. 2230, Mar. 2022.

[7] K. Krzempek et al., "CW DFB RT diode laser-based sensor for trace-gas detection of ethane using a novel compact multipass gas absorption cell," *Appl. Phys. B, Lasers Opt.*, vol. 112, no. 4, pp. 461–465, Sep. 2013.

[8] M. Graf, L. Emmenegger, and B. Tuzson, "Compact, circular, and optically stable multipass cell for mobile laser absorption spectroscopy," *Opt. Lett.*, vol. 43, no. 11, p. 2434, Jun. 2018.

[9] W. Ren, W. Jiang, and F. K. Tittel, "Single-QCL-based absorption sensor for simultaneous trace-gas detection of CH_4 and N_2O," *Appl. Phys. B, Lasers Opt.*, vol. 117, no. 1, pp. 245–251, Oct. 2014.

[10] K. Liu et al., "Highly sensitive detection of methane by near-infrared laser absorption spectroscopy using a compact dense-pattern multipass cell," *Sens. Actuators B, Chem.*, vol. 220, pp. 1000–1005, Dec. 2015.

[11] J. N. Oliaee et al., "Development of a sub-ppb resolution methane sensor using a GaSb-based DFB diode laser near 3270 nm for fugitive emission measurement," *ACS Sensors*, vol. 7, no. 2, pp. 564–572, Feb. 2022.

[12] W. Duan et al., "A laser-based multipass absorption sensor for sub-ppm detection of methane, acetylene and ammonia," *Sensors*, vol. 22, no. 2, p. 556, Jan. 2022.

[13] E. D. Hinkley, "High-resolution infrared spectroscopy with a tunable diode laser," *Appl. Phys. Lett.*, vol. 16, no. 9, pp. 351–354, 1970.

[14] D. Popa and F. Udrea, "Towards integrated mid-infrared gas sensors," *Sensors*, vol. 19, no. 9, p. 2076, May 2019.

[15] C. Li, L. Dong, C. Zheng, and F. K. Tittel, "Compact TDLAS based optical sensor for ppb-level ethane detection by use of a 3.34 μm room-temperature CW interband cascade laser," *Sens. Actuators B, Chem.*, vol. 232, pp. 188–194, Sep. 2016.

[16] H. Cui, F. Wang, Q. Huang, J. Yan, and K. Cen, "Sensitive detection of NO using a compact portable CW DFB-QCL-based WMS sensor," *Appl. Opt.*, vol. 59, no. 30, p. 9491, Oct. 2020.

[17] L. Nitzsche, J. Goldschmidt, A. Lambrecht, and J. Wöllenstein, "Two-component gas sensing with MIR dual comb spectroscopy: Fast and precise monitoring of concentrations despite complex spectra," *Tm Technisches Messen*, vol. 89, no. 1, pp. 50–59, Jan. 2022.

[18] K. Duan, M. Hu, Y. Ji, Z. Lu, S. Yao, and W. Ren, "High-temperature ammonia detection using heterodyne phase-sensitive dispersion spectroscopy at 9.06 μm," *Fuel*, vol. 325, Oct. 2022, Art. no. 124852.

[19] Q. Ren, C. Chen, Y. Wang, C. Li, and Y. Wang, "A prototype of ppbv-level midinfrared CO_2 sensor for potential application in deep-sea natural gas hydrate exploration," *IEEE Trans. Instrum. Meas.*, vol. 69, no. 9, pp. 7200–7208, Sep. 2020.

[20] Z. Lang, S. Qiao, and Y. Ma, "Acoustic microresonator based in-plane quartz-enhanced photoacoustic spectroscopy sensor with a line interaction mode," *Opt. Lett.*, vol. 47, no. 6, p. 1295, Mar. 2022.

[21] Z. Wang et al., "Doubly resonant sub-ppt photoacoustic gas detection with eight decades dynamic range," *Photoacoustics*, vol. 27, Sep. 2022, Art. no. 100387.

[22] F. Wang et al., "Wavelength scanning Q-switched fiber-ring laser intra-cavity QEPAS using a standard 32.76 kHz quartz tuning fork for acetylene detection," *Opt. Laser Technol.*, vol. 134, Feb. 2021, Art. no. 106612.

[23] Y. Liu et al., "Integrated near-infrared QEPAS sensor based on a 28 kHz quartz tuning fork for online monitoring of CO_2 in the greenhouse," *Photoacoustics*, vol. 25, Mar. 2022, Art. no. 100332.

[24] Y. Ma, Y. Hong, S. Qiao, Z. Lang, and X. Liu, "H-shaped acoustic microresonator-based quartz-enhanced photoacoustic spectroscopy," *Opt. Lett.*, vol. 47, no. 3, p. 601, Feb. 2022.

[25] F. Wang et al., "Techniques to enhance the photoacoustic signal for trace gas sensing: A review," *Sens. Actuators A, Phys.*, vol. 345, Oct. 2022, Art. no. 113807.

[26] C. Yao, S. Gao, Y. Wang, W. Jin, and W. Ren, "Heterodyne interferometric photothermal spectroscopy for gas detection in a hollow-core fiber," *Sens. Actuators B, Chem.*, vol. 346, Nov. 2021, Art. no. 130528.

[27] D. Pinto et al., "Parts-per-billion detection of carbon monoxide: A comparison between quartz-enhanced photoacoustic and photothermal spectroscopy," *Photoacoustics*, vol. 22, Jun. 2021, Art. no. 100244.

[28] Q. Wang et al., "Dual-comb photothermal spectroscopy," *Nature Commun.*, vol. 13, p. 2181, Apr. 2022.

[29] J. P. Waclawek, H. Moser, and B. Lendl, "Balanced-detection interferometric cavity-assisted photothermal spectroscopy employing an all-fiber-coupled probe laser configuration," *Opt. Exp.*, vol. 29, no. 5, p. 7794, Mar. 2021.

[30] Y. Ma, Y. He, Y. Tong, X. Yu, and F. K. Tittel, "Quartz-tuning-fork enhanced photothermal spectroscopy for ultra-high sensitive trace gas detection," *Opt. Exp.*, vol. 26, no. 24, p. 32103, Nov. 2018.

[31] X. Liu, S. Qiao, and Y. Ma, "Highly sensitive methane detection based on light-induced thermoelastic spectroscopy with a 2.33 μm diode laser and adaptive Savitzky–Golay filtering," *Opt. Exp.*, vol. 30, no. 2, p. 1304, Jan. 2022.

[32] X. Liu and Y. Ma, "Sensitive carbon monoxide detection based on light-induced thermoelastic spectroscopy with a fiber-coupled multipass cell [invited]," *Chin. Opt. Lett.*, vol. 20, no. 3, 2022, Art. no. 031201.

[33] X. Chao, J. B. Jeffries, and R. K. Hanson, "Absorption sensor for CO in combustion gases using 2.3 μm tunable diode lasers," *Meas. Sci. Technol.*, vol. 20, no. 11, Nov. 2009, Art. no. 115201.

[34] C. Zhu, P. Wang, T. Chu, F. Peng, and Y. Sun, "Second harmonic phase angle method based on WMS for background-free gas detection," *IEEE Photon. J.*, vol. 13, no. 5, pp. 1–6, Oct. 2021.

[35] F. Wang et al., "A novel wavelength modulation spectroscopy gas sensing technique with an ultra-compressed wavelength scanning bandwidth," *Spectrochimica Acta, Mol. Biomolecular Spectrosc.*, vol. 280, Nov. 2022, Art. no. 121561.

[36] H. Ghafouri-Shiraz, S. H. Lew, P. W. Tan, S. Kobayashi, I. N. Kamata, and K. Yamada, "A novel distributed feedback laser diode structure for an optical wavelength tunable filter," *Semicond. Sci. Technol.*, vol. 12, no. 9, pp. 1161–1165, Sep. 1997.

[37] R. Matthey, C. Affolderbach, and G. Mileti, "Methods and evaluation of frequency aging in distributed-feedback laser diodes for Rubidium atomic clocks," *Opt. Lett.*, vol. 36, no. 17, p. 3311, Sep. 2011.

[38] S. L. Woodward, P. Parayanthal, and U. Koren, "The effects of aging on the Bragg section of a DBR laser," *IEEE Photon. Technol. Lett.*, vol. 5, no. 7, pp. 750–752, Jul. 1993.

[39] C. Gao et al., "Self-Q-switching and passively Q-switched mode-locking of dual-wavelength Nd:YSAG laser," *Opt. Laser Technol.*, vol. 122, Feb. 2020, Art. no. 105860.

[40] S. Lv et al., "Diode-pumped continuous-wave dual-wavelength and Q-switched Yb:LuYAG lasers," *Opt. Commun.*, vol. 478, Jan. 2021, Art. no. 126356.

[41] S. Wen et al., "Dual-wavelength controllable Q-switched Nd:GSAG laser with molybdenum disulfide saturable absorber," *Infr. Phys. Technol.*, vol. 120, Jan. 2022, Art. no. 103970.

[42] Q. Wang, Z. Wang, and W. Ren, "Wavelength-stabilization-based photoacoustic spectroscopy for methane detection," *Meas. Sci. Technol.*, vol. 28, no. 6, Jun. 2017, Art. no. 065102.

[43] S. Schilt, L. Thévenaz, and P. Robert, "Wavelength modulation spectroscopy: Combined frequency and intensity laser modulation," *Appl. Opt.*, vol. 42, no. 33, p. 6728, 2003.

[44] F. Wang, J. Chang, Q. Wang, W. Wei, and Z. Qin, "TDLAS gas sensing system utilizing fiber reflector based round-trip structure: Double absorption path-length, residual amplitude modulation removal," *Sens. Actuators A, Phys.*, vol. 259, pp. 152–159, Jun. 2017.

[45] *Food and Drug Administration Code of Federal Regulations*, document 42CFR84.97, 2017.

[46] B. G. Lipták, "Instrument engineers," in *Handbook: Process Control and Optimization*, 4th ed. Boca Raton, FL, USA: CRC Press, 2003.

[47] B. Wang, X. Tang, Y. Gan, X. Li, and Y. Lu, "A TC/WMS-TDLAS mid-infrared detection method for ultra-low concentration carbon isotope methane," *J. Anal. At. Spectrometry*, vol. 37, no. 12, pp. 2615–2624, Nov. 2022.

[48] J. Dang, J. Zhang, X. Dong, L. Kong, and H. Yu, "A trace CH4 detection system based on DAS calibrated WMS technique," *Spectrochimica Acta A, Mol. Biomolecular Spectrosc.*, vol. 266, Feb. 2022, Art. no. 120418.

[49] K. Zheng et al., "Novel gas-phase sensing scheme using fiber-coupled off-axis integrated cavity output spectroscopy (FC-OA-ICOS) and cavity-reflected wavelength modulation spectroscopy (CR-WMS)," *Talanta*, vol. 213, Jun. 2020, Art. no. 120841.

[50] M. Zou, L. Sun, and X. Wang, "CH_4/C_2H_6 dual-gas sensing system based on wavelength modulation spectroscopy using a single near infrared laser," *Spectrochimica Acta A, Mol. Biomolecular Spectrosc.*, vol. 272, May 2022, Art. no. 120970.

[51] S. Shen, W. Li, M. Wang, D. Wang, Y. Li, and D. Li, "Methane near-infrared laser remote detection under non-cooperative target condition based on harmonic waveform recognition," *Infr. Phys. Technol.*, vol. 120, Jan. 2022, Art. no. 103977.

Yaopeng Cheng was born in Suzhou, China, in 2000. He is currently pursuing the B.E. degree with the College of Information Science and Engineering, Ocean University of China (OUC), Qingdao, China.

His research interests include tunable diode laser absorption spectroscopy, photoacoustic spectroscopy, and Fourier-domain optical coherent absorption spectroscopy.

Fupeng Wang received the Ph.D. degree in optical engineering from Shandong University, Jinan, China, and the University of Washington, Seattle, WA, USA, in 2019.

He is currently an Assistant Professor at the Ocean University of China, Qingdao, China. His research interests include tunable laser absorption spectroscopy (TDLAS), photoacoustic spectroscopy (PAS), nondispersive infrared spectroscopy (NDIR), and spectroscopy-based engineering applications in ocean detection and atmosphere analysis.

Jinghua Wu was born in Dezhou, Shandong, China, in 1999. He received the bachelor's degree in optoelectronic information science and engineering from the Nanyang Institute of Technology, Nanyang, China, in 2021.

He is engaged in the nondispersive infrared CO_2 sensor development and application for ocean detection.

Rui Liang was born in Shanxi, China, in October 1995. He received the B.S. degree in optoelectronic information science and engineering from the Nanyang Institute of Technology, Nanyang, Henan, China. He is currently pursuing the master's degree with the College of Physics and Optoelectronic Engineering, Ocean University of China, Qingdao, China.

His current research interests include optical sensing devices and engineering applications.

Qiang Wang received the B.S. degree in electronic science and technology and Ph.D. degree in optical engineering from Shandong University, Jinan, China, in 2011 and 2016, respectively.

After his graduate study, he worked as a Postdoctoral Fellow at the Chinese University of Hong Kong, Hong Kong, and the Max Planck Institute of Quantum Optics, Munich, Germany. He is currently a Full Professor with the State Key Laboratory of Applied Optics of Changchun Institute of Optics, Fine Mechanics and Physics, Chinese Academy of Sciences, Changchun, China. His recent research interests include laser spectroscopy, optical sensing, and engineering application of trace gas analysis in atmosphere, deep sea, and public health.

Yubin Wei received the B.S. degree in control theory and control engineering from Liaoning Petrochemical University, Fushun, China, in 2005, and the Ph.D. degree in optical engineering from Shandong University, Jinan, China, in 2016.

After his graduate study, he worked as a full-time Researcher at the Laser Institute, Shandong Academy of Sciences, Jinan, where he is currently a Full Professor. His recent research interests include laser spectroscopy, optical fiber sensing, and engineering application of trace gas analysis in coal mine safety, chemical industry, and environmental protection.

Jiachen Sun was born in Shanxi, China, in December 1995. He received the B.S. degree from Shandong University, Jinan, China, in 2018, where he is currently pursuing the Ph.D. degree with the Department of Optical Engineering, Institution of Information Science and Engineering.

He is currently major in tunable diode laser absorption spectroscopy and deep learning.

Qian Li was born in Weihai, China, in 1993. He received the B.S. degree in electrical engineering and automation engineering from the Harbin Institute of Technology (HIT), Harbin, China, in 2015, and the Ph.D. degree in circuits and systems from the Changchun Institute of Optics, Fine Mechanics and Physics, Chinese Academy of Sciences, Changchun, China, in 2010.

He is currently a Lecturer with the College of Information Science and Engineering, Ocean University of China, Qingdao, China. He is mainly engaged in weak signal detection.

Qingsheng Xue received the Ph.D. degree in optical engineering from the Changchun Institute of Optics, Fine Mechanics and Physics, Chinese Academy of Sciences, Changchun, China, in 2010.

He is currently a Professor at the Ocean University of China, Qingdao, China. His research interests include optical design, hyperspectral imaging, and development and applications of optical instruments for ocean detection.